Study on Shaking-Table Experiment of a Full-Scale Four-Story Steel Building

T. Tuan-Nam & K. Kasai
Tokyo Institute of Technology, Japan

ABSTRACT
This paper presents the dynamic collapse analysis of a full-scale four-story steel building which was experimented to collapse at the E-Defense shaking-table in Japan, in 2007, using the ground acceleration histories recorded at the JR Takatori station during the 1995 Hyogo-ken Nanbu earthquake. Deterioration of columns on the first story level due to local buckling is thought to be one of major reasons for the building collapse. Fiber method approach is adopted in the analysis to simulate local buckling at the column ends. Hypothetical analyses estimate the collapse capacity of the building specimen at approximately 0.9 times Takatori ground motion level. The collapse capacity of the building specimen under various propagating directions of the non-scaled Takatori ground motion is also investigated, showing that the building likely collapses under any propagating direction of the ground motion.

Keywords: E-Defense shaking-table, collapse experiment, numerical analysis, local buckling, fiber method approach, incremental dynamic analysis.

1. INTRODUCTION

In September 2007, a full-scale four-story steel building was experimented to collapse on the E-Defense which is the world's largest three-dimensional shake-table located in Miki City, Hyogo Prefecture, Japan. The ground acceleration histories recorded at the JR Takatori station during the 1995 Hyogo-ken Nanbu earthquake were used as the input for the shake-table experiments under various scales. Experimental result shows that collapse occurred under the 100% Takatori motion, due to local buckling leading to deterioration of columns in the first story level (Fig. 1).

Figure 1. Collapse of the building specimen after the experiment

Collapse behavior of the building in this experiment has attracted a lot of researchers to study and establish an effective model for simulating the collapse manner. However, behavior of the specimen involving yielding and local buckling of columns is still very difficult to simulate. The study deals with establishing a simple analytical model of the building specimen addressing that key point. Fiber method approach was adopted to simulate local buckling behavior of column members. The analytical model consists of both structural and non-structural components. Dynamic responses of the frame model subjected to the same input ground motions as those adopted in the test are analysed and compared to experimental data. Collapse mechanism is analytically interpreted, and hypothetical analyses for evaluating collapse capacity of the building specimen are also carried out.

2. BUILDING SPECIMEN

The building specimen is a full-scale 4-story steel moment frame with concrete slabs and autoclaved aerated concrete (ALC) panels for exterior walls. The plan dimension is 6 m × 10 m, and the total height from the upper surface of stiff foundation is about 14 m. Wide-flange sections are used for beams and hollow square sections are used for columns. Steel material type is SN400B for beams and BCR295 for columns. Section shapes are given in Table 2.1.

Table 2.1. Sections and materials of the steel frame

	Beam (SN400B)			Column (BCR295)
Story	G1	G11	G12	C1,C2
4	H-346×174×6×9	H-346×174×6×9	H-346×174×6×9	RHS-300×9
3	H-350×175×7×11	H-350×175×7×11	H-350×175×9×14	RHS-300×9
2	H-396×199×7×11	H-400×200×8×13	H-400×200×8×13	RHS-300×9
1	H-400×200×8×13	H-400×200×8×13	H-390×200×10×16	RHS-300×9

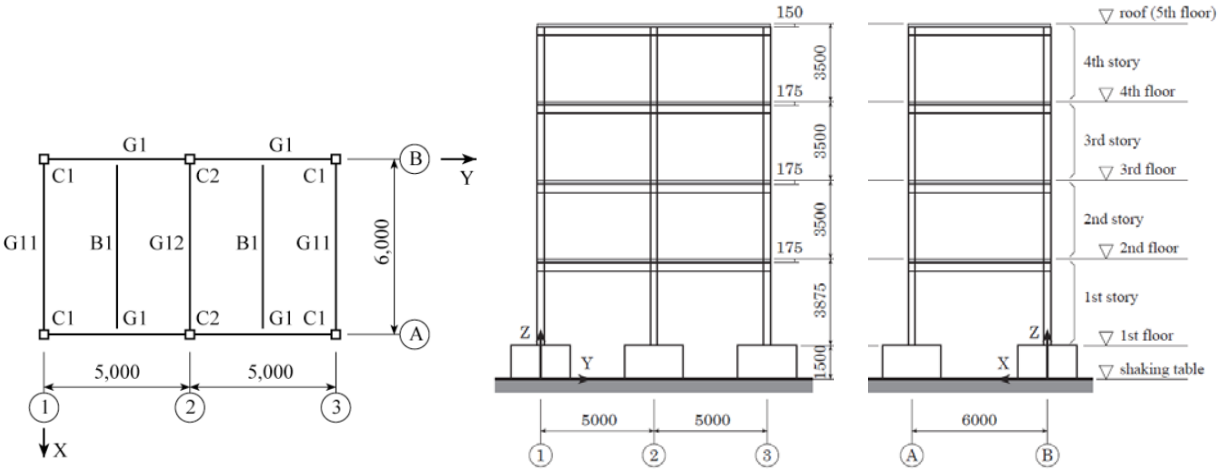

PLAN ELEVATION

Figure 2. Framing plan and elevation of the building specimen

3. MODELING FEATURES

3.1. General modeling

The building specimen is numerically simulated by PC-ANSR analysis program, using a three-dimensional model composed of various frame members, such as beams, columns, panel zones, column base plates, and others (Fig. 3-a). Slab diaphragm is adopted by using truss bars, thus in-plane displacements of all nodes at the same floor level are equal. Composite action of the steel beam and concrete slab is taken into account.

Column-base is modeled as elastic rotational spring. Rotational stiffness of column-base is obtained following AIJ specification as Eqn. 2.1 where, E: Young's modulus, n_t: number of bolts in tensile side, A_b: sectional area of an anchor bolt, d_t: horizontal distance from column-center to center of anchor bolts in tensile side, d_c: half of column depth, l_b: anchor bolt length.

$$K_b = \frac{En_t A_b \left(d_t + d_c\right)^2}{2l_b} \tag{2.1}$$

The beam-to-column panel zone tends to deform in shape of parallelogram where one diagonal direction is in tension and the other is in compression; besides right angles at the joints between beam/column-end and panel remains right angles (Fig. 3-b). Shear strain causes the panel to rotate at certain angle; thus the panel can be considered to work as a rotational spring.

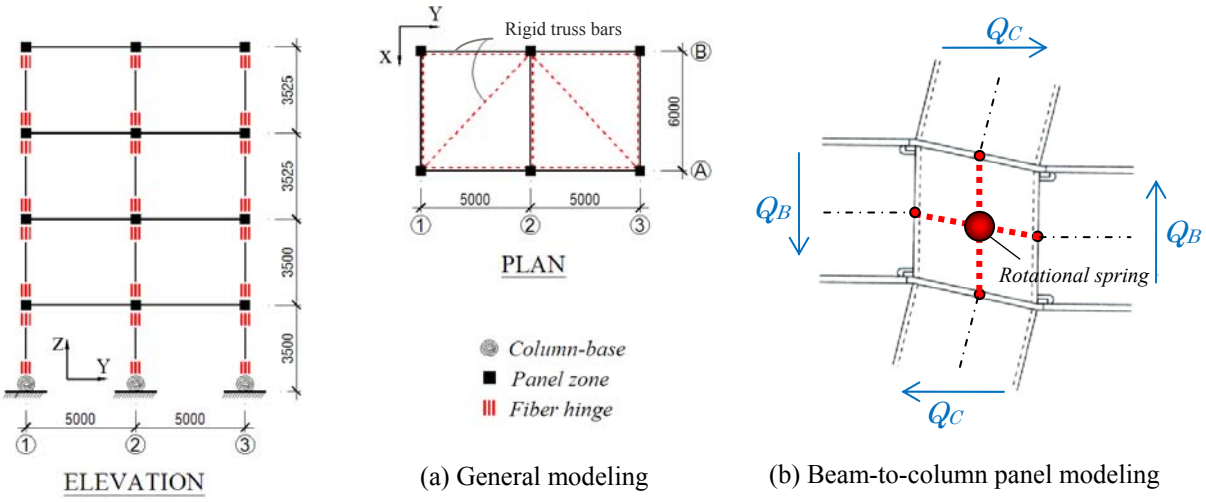

(a) General modeling (b) Beam-to-column panel modeling

Figure 3. Three-dimensional analytical model of the building specimen

3.2. Modeling of column hinges

3.2.1. Fiber method approach

Fiber method approach was employed in this study, where the column end is modeled as a 'fiber hinge element' composed of two rigid plates connected by fibers distributed over the cross section (Fig. 4-a). The hinge zone is modeled to have a zero length, which means its two end nodes must have the same coordinates. Its rotation characteristic is achieved by finite length of buckling zone (Fig. 4-b).

The nonlinear stress-strain properties of 'fiber element' which are based on this finite length is illustrated in Fig. 4-c, where σ_y^+ and σ_y^- represent nominal yield stress due to tension and nominal buckling stress due to compression, respectively; $\varepsilon_1, \varepsilon_2, \varepsilon_3$ are negative strains associated with each gradually reduced buckling stiffness of the element; and α, β, γ are factors used to define the stresses corresponding to some control points on the curve.

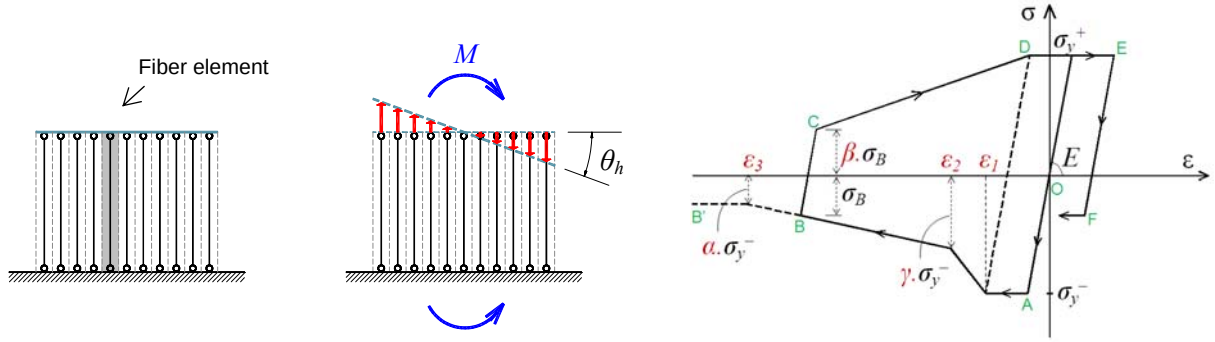

(a) Hinge model (b) Rotation characteristic (c) Hysteretic behavior of fiber elements

Figure 4. Structural model of column hinge element

The first zone O-A is associated with the initial loading of the element which approaches the critical buckling stress (assumed to be equal to yield stress) at point A. Zone A-B is characterized by a decreasing load accompanied by element shortening and buckling. Zone B-C-D is the compression unloading and tensile loading of the fiber element. Subsequent hysteretic loops have the same characteristic except that the consecutive peak compressive stresses are reduced due to deterioration caused by the previous inelastic cycling of the material. Hence, the compressive yield stress at point F, where the element begins to yield in compression, is set equal to the value of compressive stress at point B. Point B is named for the reversal location of the curve when the element shortening stops. This location changes per load cycle. Accordingly, the curve continues to approach point B and thereafter along zone B-B'.

3.2.2. Influence of fiber hinges on column stiffness

Fiber hinges are added at both top and bottom ends of every column. Finite length *l* of the hinge evidently changes column bending stiffness. Thus, the column needs to be stiffened in order to eliminate the additional flexibility due to fiber hinges.

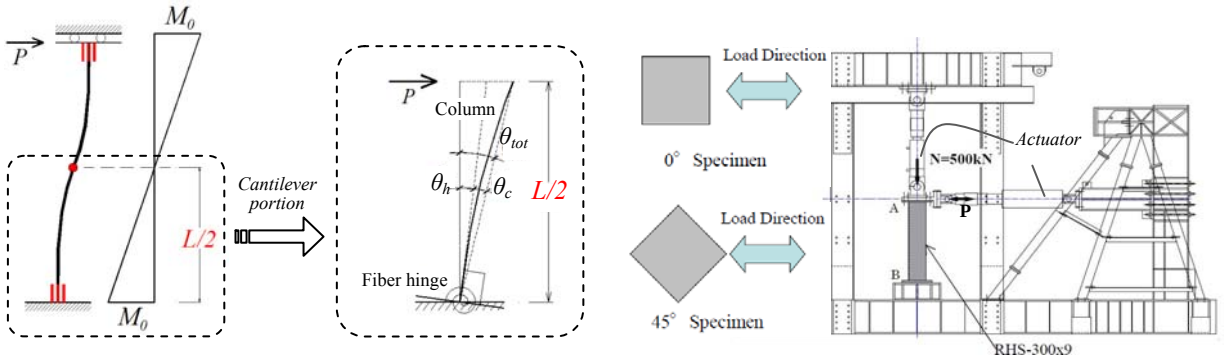

(a) Column modeling with fiber hinge added (b) Cantilever column bending test setup

Figure 5. Influence of fiber hinges on column stiffness

At each floor level, columns are considered to work as the model shown in Fig. 5, where both column ends are restrained from rotation but top end allowed to translate. In such manner, the column (length *L*) is supposed to consist of two cantilever column portions joining at the inflection point which generally locates at the mid-height of the column. The column portion is stiffened by changing its Young's modulus of elasticity, *E,* to a fictitious value, *E'*.

$$E' = E.\frac{L/2}{L/2 - 3l} = E.\frac{L}{L - 6l} \tag{3.2}$$

By equating the deflection of the cantilever portion (length *L/2*) induced by both hinge rotation and column elastic rotation with theoretical value, Eqn. 3.2 is obtained. The effect of this stiffness modification is shown up on the moment vs. chord rotation relationship of the cantilever column (Fig. 6). The analytical results almost match the experimental data.

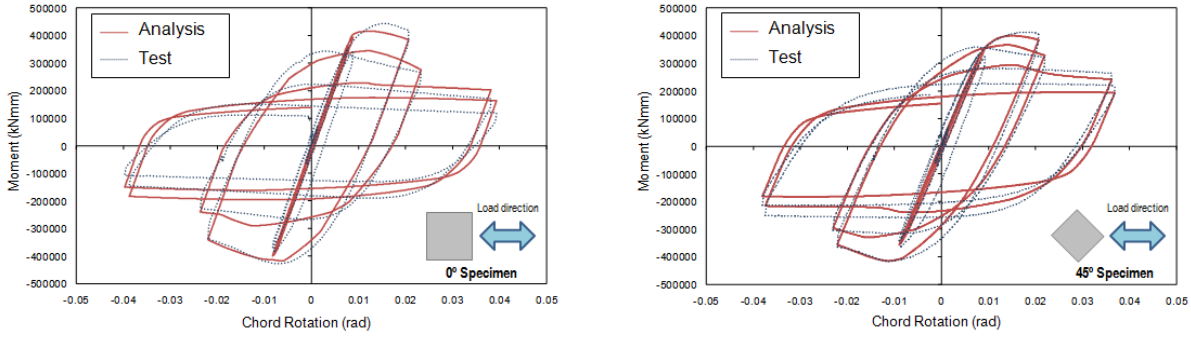

Figure 6. Cantilever column hysteretic behavior

3.3. Modeling of non-structural components

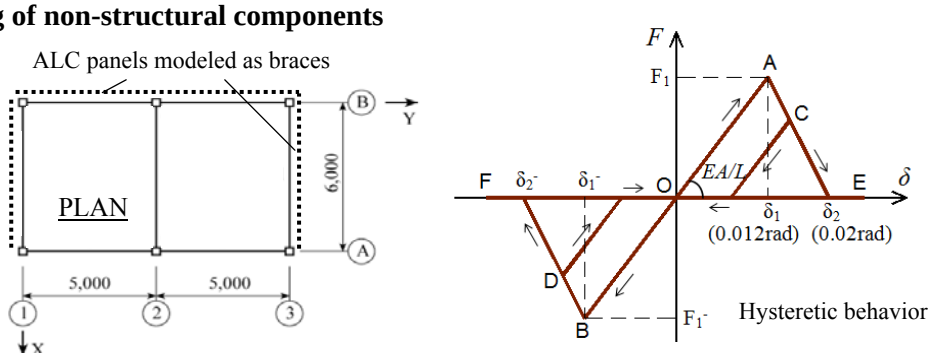

Figure 7. ALC external walls modeled as braces with slip behavior

Non-structural components are simulated using braces added on three exterior frames of the building, as shown in Fig. 7 with slip behavior so as to degrade resistant capacity after the story drift angle overpassed 0.012 rad and be completely damaged under the story drift angle of 0.02 rad. These components contribute about 10% lateral stiffness at each story. Elastic stiffness of non-structural components on each story which is determined by the subtraction of frame stiffness from stiffness of the whole building is then distributed to each brace.

4. TIME-HISTORY ANALYSIS

Rayleigh damping is considered in the analysis, and damping ratio of 2% is assigned to cover the first two fundamental modes in both translational directions. It is noteworthy that due to counting for stiffness of nonstructural components, the obtained vibration periods (shown in Table 4.1) are consistent with those from the free vibration test of the building specimen which are 0.8 sec in X direction and 0.76 sec in Y direction (Yamada et al).

Table 4.1. Fundamental periods [sec]

Mode	X-dir.	Y-dir.
1	0.79	0.76
2	0.25	0.24

Actual acceleration records measured on the shaking-table during the test are adopted as the input acceleration in the analyses. EW, NS and UD components are used for the X, Y and Z directions, respectively. Three analysis cases of excitation levels, including 20%, 60% and 100% Takatori ground motions, are presented.

Subjected to the motion of 20% Takatori record, the building has worked elastically. The ground motion which is equal to Level-1 design earthquake is not strong enough to separate the base plate away from the stiff foundation. There is hence little likelihood that pre-tension force of anchor bolts is overcome. Thus, the column base under this elastic load case is considered to be very stiff. The analysis output almost agrees with that recorded in the experiment, as shown in Fig. 8.

Fig. 8-a shows the time-history curves of story drift angle of the first story level in X and Y directions. The orbit of story drift angles is also plotted. Figs. 8-b,c show the story shear (Q) vs. story drift angle (r) relation of the first story in X and Y directions, respectively. In those plots, solid lines stand for the analytical results, and broken lines show the experimental records provided by the Building Collapse Simulation Working Group. Those figures show good agreement between the analytical results and experimental records.

Under the 60% Takatori ground motion which is 1.5 times larger than the Japanese Level-2 design earthquake (i.e. peak ground velocity at 0.75 m/s), the building performed inelastic behavior. Figs. 9-a,b,c show the analytical results for the collapse excitation level in the same arrangement as those of 20% Takatori presented above.

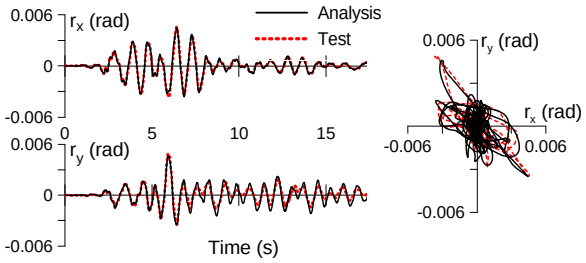

(a) Story drift angle time-history & orbit

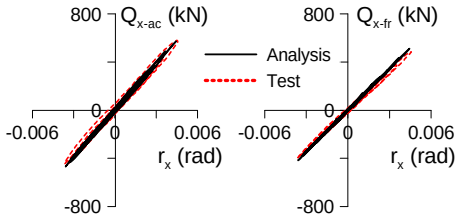

(b) Story shear vs. story drift angle (X-dir)

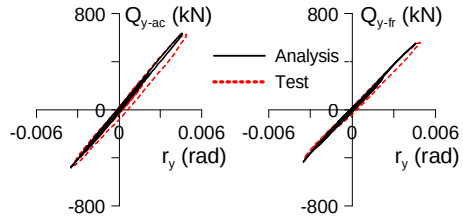

(c) Story shear vs. story drift angle (Y-dir)

Figure 8. Analysis results (20% Takatori, 1st story)

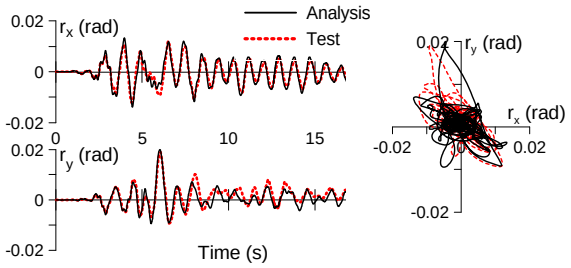

(a) Story drift angle time-history & orbit

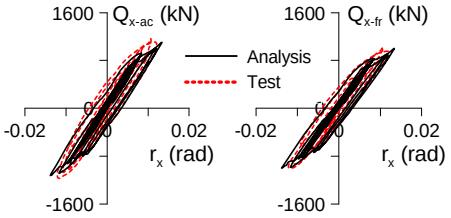

(b) Story shear vs. story drift angle (X-dir)

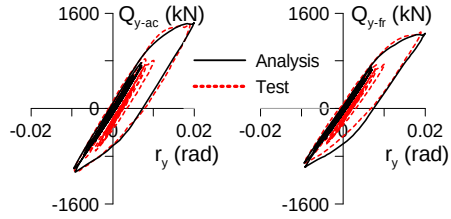

(c) Story shear vs. story drift angle (Y-dir)

Figure 9. Analysis results (60% Takatori, 1st story)

Since non-structural components are taken into consideration in this study, the analytical model is capable of capturing the difference between the acceleration-based story shear (Q_{ac} – obtained from inertial force of the building) and the frame-based story shear (Q_{fr} – obtained from column restoring forces), as shown in the figures, demonstrating the certain contribution of non-structural components in lateral stiffness of the building.

The collapse occurred when the building was subjected to the 100% Takatori ground motion which is 2.5 times larger than Level-2 design earthquake (i.e. peak ground velocity at 1.28 m/s). Fig. 10 shows the analytical results for the collapse excitation level. The model shows good accuracy of story deformation time-history curves in comparison with experimental data. Target collapse story drift angle of the first story in either X or Y direction is almost achieved, which is 0.080 rad and 0.186 rad, respectively (Suita et al). Deterioration of column strength due to local buckling characterized by negative slope in the plot of story shear - drift angle relation (Fig. 10-b) also shows up significantly, leading the specimen to collapse.

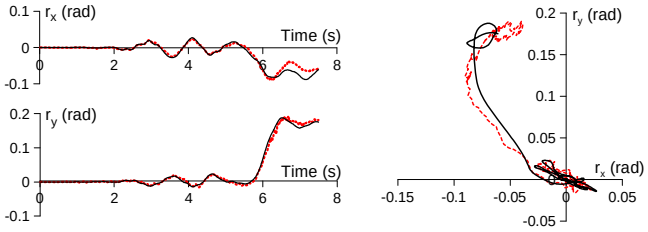

(a) Story drift angle time-history & orbit

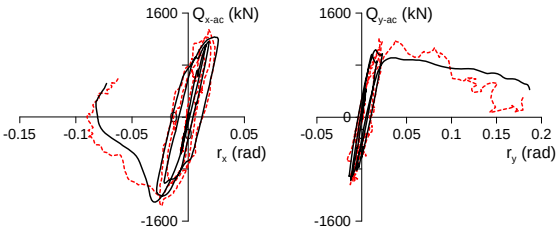

(b) Story shear vs. story drift angle

Figure 10. Time-history analysis results (100% Takatori excitation level, 1st story)

5. COLLAPSE CAPACITY ANALYSIS

After collapse behavior was achieved for the 100% Takatori excitation level, additional analyses for determining the collapse capacity of the specimen building and hypothetical investigation of the building response under various directions of the same excitation level are carried out.

5.1 Hypothetical analysis

The input ground motion of non-scaled Takatori acceleration record that was used in the collapse experiment is adopted. In these analyses, behavior of the analytical model is numerically examined under the changes of earthquake load direction.

The EW and NS components of the Takatori record which are used previously for X and Y directions (denoted by $\ddot{u}_{gx}$ and $\ddot{u}_{gy}$ in Fig. 11-a, respectively) are rotated at a counterclockwise angle of α with respect to the original ones. 12 analysis cases in accordance with 12 different load directions (i.e. α varies respectively from 0°, 30°, 60°... to 330°) are carried out. Input accelerations are computed from the original components as follows:

$$\ddot{u}_{gx-input} = \ddot{u}_{gx}\cos\alpha - \ddot{u}_{gy}\sin\alpha \quad (5.1)$$

$$\ddot{u}_{gy-input} = \ddot{u}_{gx}\sin\alpha + \ddot{u}_{gy}\cos\alpha \quad (5.2)$$

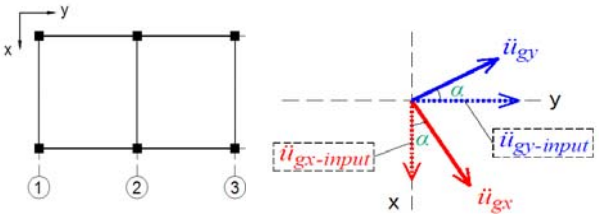

(a) Rotation of input earthquake acceleration

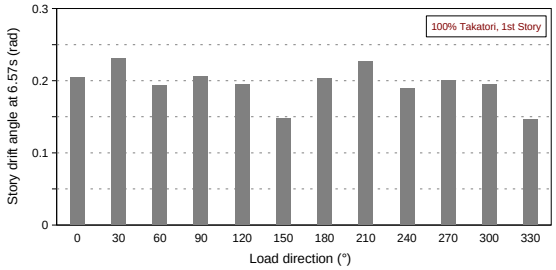

(b) SRSS story drift angle

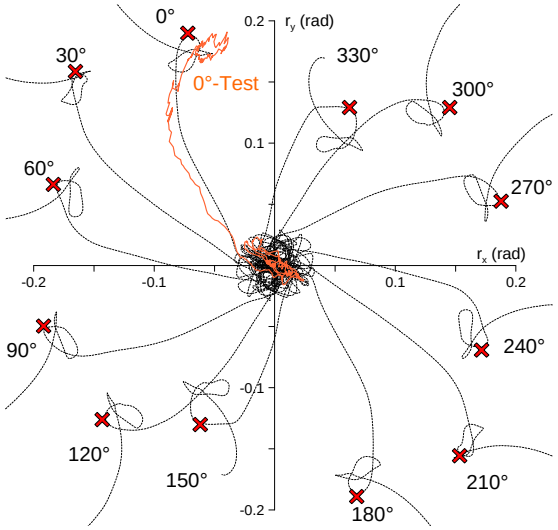

(c) Story drift orbit (1st story)

Figure 11. Hypothetical analysis results

Fig. 11-c presents the story drift orbits for all analysis cases, where '×' symbols mark the moment of 6.57 sec that is the 'collapse instant' recorded in the experiment (Suita et al, 2008). Story drift angle values obtained at this instant per each case are compared with one another, illustrated in Fig. 11-b. Dealt with story drift angle values, a new value of 'SRSS drift angle' is proposed with the meaning of square root of sum of squares of drift angle in X and Y direction (i.e. r_x, r_y) at certain time, regardless of direction, i.e. $r_{SRSS}(t) = \left(r_x^2(t) + r_y^2(t)\right)^{1/2}$ (5.3).

Analytical results show that the model likely exceeds 'collapse level' defined according to the Blind Analysis Contest rule (i.e. story drift angle exceeds ±0.13 rad) in all cases. Nevertheless, there are only a few cases where the model attains the same displacement as recorded in the experiment (i.e. story drift angle reaches ±0.19 rad). In accordance with the changing of load orientation, the most vulnerable load cases where r_x reaches ±0.20 rad correspond to the value of α varied from +30° to +120°. Such vulnerable cases for r_y correspond to the value of α varied from 0° to +30°.

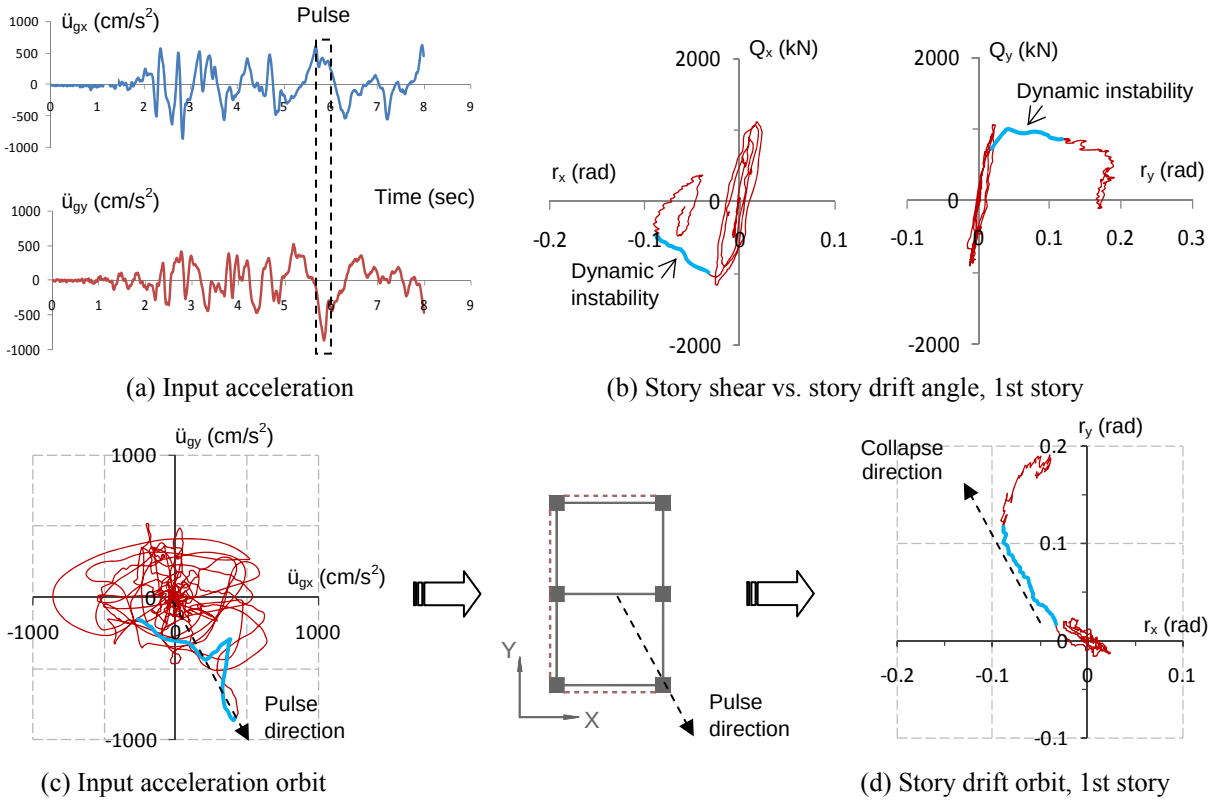

(a) Input acceleration

(b) Story shear vs. story drift angle, 1st story

(c) Input acceleration orbit

(d) Story drift orbit, 1st story

Figure 12. Collapse manner of the building specimen observed in the experiment

In order to figure out the reason for the difference about responses of the model among various cases, collapse direction of the building is analyzed in accordance with the input ground motion. Firtsly, collapse direction is defined based on the orbit of the building displacement. The building tends to collapse whenever the dynamic instability induced by P-delta effect shows up significantly (as shown by the solid line in Fig. 12-b). Based on that time range in the story drift orbit plot, one can estimate the collapse direction (Fig. 12-d). Figs. 12-a,c show the pulse direction of the input ground motion which is coincident with the collapse direction of the building.

In accordance with the changing of the input acceleration orientation, the collapse direction also changes. As a matter of fact, this building specimen is 1.05~1.10 times stiffer in longitudinal side (Y dir.) than in transverse side (X dir.). Thus, it may be explained that if the collapse direction matches Y dir. (e.g. α approximates -30° or +150°), the probable maximum deformation of the building is less than in other cases, as can be seen in Fig. 11-c.

In summary, collapse capability of the building specimen is influenced by the following factors: collapse direction and column strength direction. In case the shaking direction of ground motion is along the longitudinal side of the building specimen (i.e. in what side the building is stiffer), the building likely may resist better to collapse. On the other hand, for the building having box columns, if the collapse direction is diagonal with respect to the column section (i.e. in what side the column is weaker), degradation may occur in columns more likely than other sides, consequently leading to the instability and collapse of the whole structure.

5.2 Incremental dynamic analysis

Incremental dynamic analysis (IDA) is carried out to the numerical model in which the intensity of the ground motion selected for collapse investigation is incrementally increased until the global collapse capacity of the structure is attained. Peak story drift angle per scale factor is marked by red circles in Figs. 16-a,b.

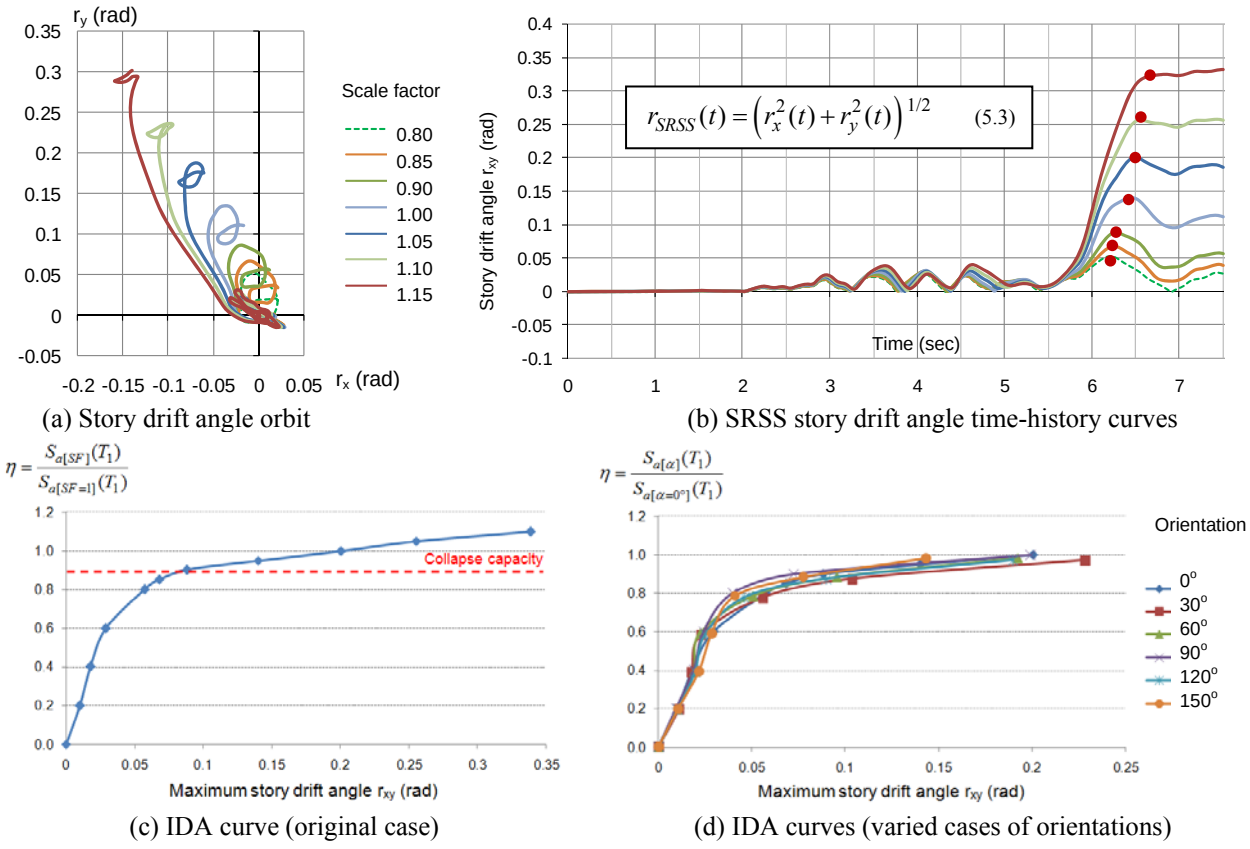

Figure 13. Incremental dynamic analysis results

The IDA curve is shown in Fig. 16-c, in which the abscissa indicates peak story drift ratio that normally obtained from the first story, and the ordinate stands for normalized spectral acceleration at natural period $S_a(T_1)$ (also equal to scale factor), which is the ratio of $S_{a[SF]}(T_1)$ in case of scaled motion to $S_{a[SF=1]}(T_1)$ in case of non-scaled motion.

The global collapse capacity is considered reached when the curve in this plot becomes flat. That is, when a small increase in the ground motion intensity generates a large increase in the structural response. However, since infinity is not a possible numerical result, FEMA 350 (2000) suggested the 20% tangent slope approach, in which the last point on the curve with a tangent slope equal to 20% of the slope in the elastic region is defined to be the capacity point. Using the 20% tangent slope approach, results from incremental dynamic analyses estimate the collapse capacity of the building specimen at approximately 90% Takatori ground motion level.

The collapse capacity of the building specimen under various propagating directions of the 100% Takatori ground motion is also investigated. The EW and NS components of the Takatori record which are used previously for X and Y directions are rotated at an angle of α with respect to the original ones. SRSS story drift and SRSS spectral acceleration are adopted, in which SRSS stands for square root of sum of squares of the parameters in X and Y directions at specific time. The incremental dynamic analysis curves are shown in Fig. 13, in which the ordinate represents normalized spectral acceleration which is the ratio of spectral acceleration obtained from the direction-rotated ground motion to spectral acceleration estimated from the original ground motion, almost equal to scale factor of ground motion. Results from the curves show that collapse capacity of the building specimen under various load cases is almost equivalent to the original case (i.e. α = 0). It thus can be concluded that the building likely collapses under any propagating direction of the 100% Takatori ground motion.

6. CONCLUSION

Numerical simulation and collapse dynamic analysis of the E-Defense four-story steel building were summarized in this paper. Followings are some concluding remarks:

(1) Fiber element based method which is adopted in the study is a simple approach but takes effect in modeling local buckling at the column ends, one of the major reasons of building collapse.
(2) The analytical model is successful in simulating dynamic inelastic response and collapse manner of the building which is supposed to be the deterioration of column strength due to local buckling.
(3) Hypothetical analyses show that under any orientation of the original input ground motion, the building likely collapses with the same collapse manner as recorded in the experiment in spite of different biaxial bending effects among cases of orientation.
(4) Collapse capacity of the building specimen is estimated at approximately 0.9 times the original Takatori ground motion.

ACKNOWLEDGEMENT
The authors acknowledge Dr. Bruce F. Maison (California, USA), Dr. Troy A. Morgan (Tokyo Institute of Technology, Japan) and Prof. Tada Motohide (Osaka University, Japan) for their enthusiastic technical supports.

REFERENCES

FEMA (2000). Recommended Seismic Design Criteria for New Steel Moment-Frame Buildings. **Publ. No. 350**, ASCE, Federal Emergency Management Agency, Washington DC.

Maison, B. F., and Popov, E. P. (1980). Cyclic Response Prediction for Braced Steel Frames. *Journal of the Structural Division,* ASCE, **Vol. 106**, No. ST7, pp.1401-1416.

Yamada, S., Suita, K., Tada, M., Kasai, K., Matsuoka, Y., and Shimada, Y. (2008). Collapse Experiment on 4-Story Steel Moment Frame: Part 1 Outline of Test Results. *The 14th World Conference on Earthquake Engineering*.

Suita, K., Yamada, S., Tada, M., Kasai, K., Matsuoka, Y., and Shimada, Y. (2008). Collapse Experiment on 4-Story Steel Moment Frame: Part 2 Details of Collapse Behavior. *The 14th World Conference on Earthquake Engineering*.

Tada, M., Tamai, H., Ohgami, K., Kuwahara, S., and Horimoto, A. (2008). Analytical Simulation Utilizing Collaborative Structural Analysis System. *The 14th World Conference on Earthquake Engineering*.